UV-curable adhesive microsphere whispering gallery mode resonators

Guoqiang Gu (顾国强)[1,2], Lujian Chen (陈鹭剑)[1], Hongyan Fu (付宏燕)[1], Kaijun Che (车凯军)[1], Zhiping Cai (蔡志平)[1], and Huiying Xu (许惠英)[1*]

[1]*Institute of Optoelectronic Technology, School of Information Science and Engineering, Xiamen University, Xiamen 361005, China*

[2]*Science and Technology on Electronic Information Control Laboratory, Chengdu 610036, China*

[*]*Corresponding author: xuhy@xmu.edu.cn*

Received May 25, 2013; accepted September 4, 2013; posted online September 30, 2013

We report the fabrication and optical characterization of spherical whispering gallery mode (WGM) resonators made from ultraviolet (UV)-curable adhesive. The fabricated microspheres have good sphericity and surface smoothness, and can directly adhere to the tip of half-tapered fibers for easy manipulation. WGMs are efficiently excited in the microsphere using an evanescent field of the tapered silica optical fibers. Resonances with quality factors of 1.3×10^5 are observed. The dependence of wavelength shifts of WGM resonances on the input light powers shows that the resonant wavelength of the proposed microsphere resonators can be tuned thermo-optically.

OCIS codes: 140.4780, 160.6840, 230.4000, 260.5740.
doi: 10.3788/COL201311.101401.

Optical cavities that can circularly confine electromagnetic oscillation inside a smooth inner surface with a stable field distribution because of continuous total internal reflection are called whispering gallery mode resonators (WGMRs). The cavity modes are referred to as morphology-dependent resonances[1], which are a function of cavity morphological characteristics and dielectric properties. These WGMRs can be realized from a wide variety of materials (from liquid to solid) in numerous kinds of structures, such as microspheres, microtoroids, and microdisks, up to the most exotic structures (i.e., microbottle and micro-kayak)[2−4]. Spherical dielectric resonators are the simplest three-dimensional (3D) WGMRs, typically with diameters of tens to hundreds of micrometers. They have elicited increasing research attention over the past few decades because of their exceptionally high-quality factors (Q-factor), ease of fabrication, and small mode volume[5,6].

WGM resonances were initially observed in light scattering from spherical dielectric particles in liquid resonators[7]. Lasers were originally implemented in these microdroplets[8]. Microdroplets were also used in studies of cavity-enhanced spectroscopy[9], dye-doped liquid lasing, fluorescence[10,11], and stimulated Raman scattering[12]. Unfortunately, applications of microdroplet WGMRs are greatly limited by their short evaporative lifetime, mechanical instabilities, and difficulties in manipulation. One of the most common production techniques is to solidify droplets of molten silica into solid microspheres[13]. This widely used technique produces microspheres with the desired diameter by heating the tip of a tapered optical fiber in the focused beam of a CO_2 laser. The preparation of silica microspheres with CO_2 laser not only requires glass in the form of a rod or a fiber and permits the fabrication of only one microsphere at a time, but also requires a complex setup involving a high-power CO_2 laser. Polydimethylsiloxane (PDMS) is a material of high light transmittance, distinct thermal response, and large thermal nonlinearity. PDMS is extensively used to fabricate microspheres[14] and investigate electromagnetically induced, transparency-like effect and thermal sensing of the microcavities[15−17]. However, the cure time of a PDMS microsphere is over a period of 4 or 5 days at room temperature. Other polymer microspheres can be prepared by melting–solidifying or heterogeneous polymerization methods with polymethyl methacrylate[18] and dye-doped polymer[19]. Nevertheless, the surface smoothness and Q-factor of these microspheres may be restricted to a certain degree because of uneven heating and introduction of other impurities.

In this letter, we demonstrate a simple, reliable, and time-saving method to fabricate high-quality microsphere WGMRs in low-loss, ultraviolet (UV)-curable adhesive with a low-cost UV lamp. The fabricated microspheres possess good sphericity and surface smoothness, and directly adhere to the tip of half-tapered fibers for easy

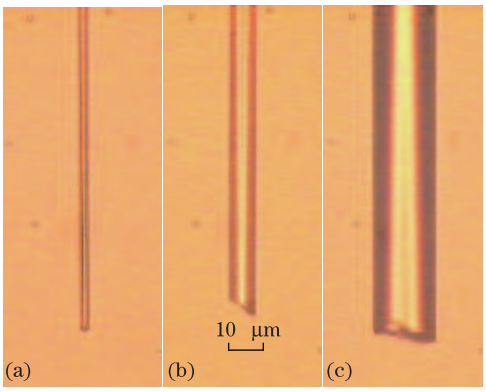

Fig. 1. Microscope images of three half-tapered fibers with waist diameters of (a) 3.2 μm, (b) 8.6 μm, and (c) 20 μm under a 40× microscope objective.

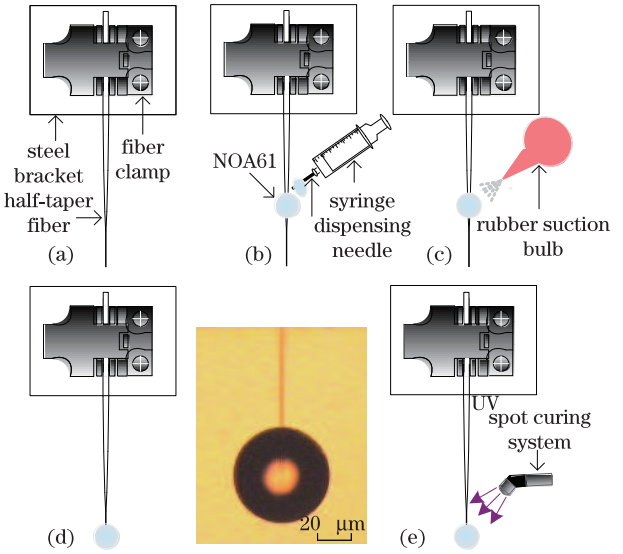

Fig. 2. (a–e) Fabrication process for obtaining UV-curable adhesive microspheres. Inset: microscope image of a UV-curable adhesive microsphere with diameter $D \sim 81.4$ μm under a 10× microscope objective.

manipulation. Meanwhile, using UV-curable photopolymers with a UV lamp allows parallel fabrication of several spheres at a time, and the preparation time is less than half an hour. The WGM resonances of the UV-curable adhesive microspheres have been characterized using evanescent coupling from tapered silica optical fibers. High Q-factors of the resonances at wavelengths near 1.55 μm have been observed. The dependence of the wavelength shift of WGM resonances on input light power has also been studied, and results show thermo-optically controllable resonance of UV-curable adhesive microsphere WGMRs.

The microsphere is fabricated from a droplet of commercially available Norland Optical Adhesive 61 (NOA 61) transferred onto an already fabricated half-tapered optical fiber using a heating-and-pulling technique. Figure 1 shows the half-tapered fiber with waist diameters of 3.2, 8.6, and 20 μm.

NOA 61 was chosen for microsphere fabrication because of its extremely broad transparency, good chemical stability, appropriate viscosity (300 cps at 25 $^\circ$C), high hardness (after curing), low shrinkage, thermal nonlinearity, and excellent curability upon UV irradiation[20]. Its low optical attenuation loss in the range from 400 to 2000 nm is also the basic requirement to obtain high-Q WGMRs working at optical communication band. The absorption loss of NOA 61 in the 1550-nm wavelength band is estimated to be 0.42 dB/cm. The transmission of NOA 61 was measured using a Lambda 750 UV/VIS spectrometer.

Figure 2 shows a schematic diagram of the fabrication process for the UV-curable adhesive microsphere.

Firstly, a half-tapered fiber with a proper length was fixed onto a fiber clamp that was vertically mounted on a steel bracket (Fig. 2(a)). We then used a high-precision dispensing needle to transfer the NOA 61 droplets onto the taper transition of the half-tapered fiber, forming microdroplets with diameters of around tens or hundreds of microns (Fig. 2(b)). The dispensing needles were primarily coated with a certain amount of NOA 61 droplets and inserted into a syringe to conveniently manipulate them. Owing to the strong surface tension, the microdroplet that stuck to the taper transition possesses perfect spherical shape and smooth interface. Next, a rubber suction bulb was used to blow and slide the microdroplet from the taper transition to the taper waist (Fig. 2(c)). Considering that NOA 61 has a particular viscosity, the liquid microdroplet can maintain its size and spherical shape during the blowing process. In the taper waist region, the microdroplet fell slowly under gravity along the smooth and symmetric microfiber, and then stopped in the fracture area of the half-tapered fiber (Fig. 2(d)).

An ideal UV spot-curing system (ELC-410) with a UV intensity output of 90 mW/cm^2 at 365 nm was used to obtain the solid microsphere. The high hardness and low shrinkage natures of NOA 61 combined with appropriate UV exposure time ensured that the microdroplets cure into solid microspheres with almost no deformation (Fig. 2(e)). During the experiment, the exposure time of about 8 to 10 minutes at room temperature has been proven to be the best time for producing microspheres with excellent sphericity, unchanged geometry, and sufficient hardness. Adequate hardness prevents microsphere damage caused by the taper fiber in other processes. The microsphere adhered to the tip of the half-tapered fiber that was used as a stem to position the microsphere. Several microspheres were simultaneously fabricated when we fixed some of the microdroplets that stuck to the half-tapered fibers on another steel bracket. The inset in Fig. 2 shows a microscope image of an optical adhesive microsphere with a diameter (D) of 81.4 μm.

The experimental setup to characterize the WGM resonances of the adhesive microsphere is shown in Fig. 3. A broadband light source of continuous wave (CW) output centered at 1549 nm and a spectral width of 56.28 nm was used to excite the WGMs. As described above, a tapered silica fiber fixed on a U-shaped aluminum sheet and connected to the light source was used to couple light in and out of the microsphere using the evanescent field coupling technique[21]. The microsphere and its holder were mounted on a compact fiber-clamping fixture. The positions of the sphere and the tapered fiber were monitored from the side and top using microscopes equipped with charge-coupled device (CCD) cameras. The side and top views of the microsphere with a diameter of 160.6 μm are shown in the upper left and right corner of Fig. 3. The separation between the microsphere and the tapered fiber was controlled by a precision nanotranslation stage and

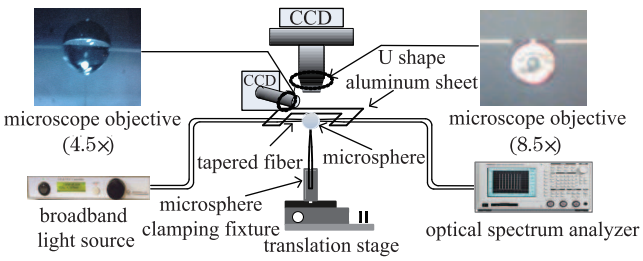

Fig. 3. Experimental setup used for microsphere resonance characterization.

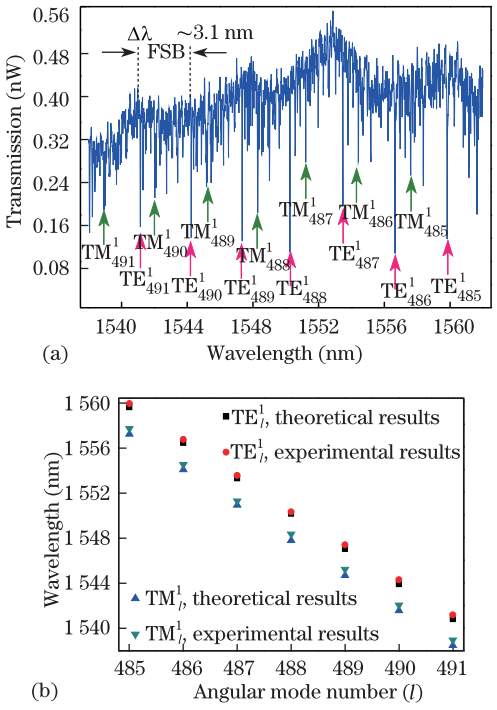

Fig. 4. (a) Experimental resonance spectrum for wavelengths between 1538 and 1562 nm for the microsphere ($D \sim 160.6$ μm); (b) calculated results of resonant TE and TM WGMs with radial order i =1 and angular mode number l = 485–491 compared with experiment results. FSR: free spectral range.

equipped with piezoelectric actuators stepper motors. The power of the output light transmitted through the tapered fiber was coupled into an optical spectrum analyzer (OSA), and the transmission spectrum was recorded.

Figure 4(a) shows the resonance spectrum of a microsphere resonator with a diameter of 160.6 μm at the position of the equatorial plane through a tapered coupling fiber with a waist diameter of 1.6 μm. A clearly dense spectral in the power transmission was observed. The emergence of many higher-order radial modes and nondegenerate, higher-order angular modes is attributed to the microsphere eccentricity and the refractive index mismatch between the silica taper and the adhesive microsphere. The theoretical values of free spectral range (FSR) can be estimated using

$$\Delta\lambda_{\mathrm{FSR}} \approx \lambda^2/(2\pi na), \tag{1}$$

where $\Delta\lambda_{\mathrm{FSR}}$ is the FSR of the two modes with the same radial order (i) and the same polarization but with the adjacent angular mode number (l), λ is the wavelength at which a resonance occurs, and n and a are refractive index and radius of the microsphere, respectively. $\lambda \sim 1.55$ μm, $a \sim 80.3$ μm, and the refractive index of NOA61 adhesive microsphere at 1.55 μm is $n \sim 1.542$[20]. Thus, $\Delta\lambda_{FSR}$ is estimated to be 3.09 nm. The FSR of our fabricated microsphere was measured to be 3.10 nm, which agrees well with the theoretical estimation.

We theoretically calculated the resonance positions of the microsphere. When considering a large sphere with the radial order i=1 and the angular mode number $l \geq 1$, the positions of the transverse electric (TE) and transverse magnetic (TM) resonance WGMs can be given asymptotically as[1]

$$nk_{l,i}a = v + 2^{-1/3}\alpha_i v^{1/3} - \frac{P}{(n^2-1)^{1/2}} + o(v^{-1/3}), \tag{2}$$

where ν=l+1/2, α_i is the ith root of the Airy function [Ai(-z)], k is the wave vector, and

$$P = \begin{cases} n & \text{for TE modes} \\ 1/n & \text{for TM modes.} \end{cases}$$

The values of the resonant TE and TM modes for i=1 and l=485–491 marked in Fig. 4(a) can be determined by identifying the resonance features with Eq. (2). Comparisons between the experimental and theoretical results show good agreement, as illustrated in Fig. 4(b). The relative errors of these resonant TE and TM WGMs between the calculation results and the measurement data are less than 0.04%.

The normalized transmission intensity as a function of wavelength is shown in Fig. 5. The highest coupling efficiency measured in this experiment is about 72.6 %. This value is lower than the taper-microsphere (silica–silica) coupling system in Ref. [21], but higher than the coupling efficiency of the silica optical fiber taper and the Germanium microsphere in Ref. [22]. According to the coupled mode theory, the coupling efficiency is strongly related to the phase-match condition. Modes that have larger phase-match experience stronger coupling. During the characterization of the WGM resonances, we also found that the taper easily adheres to the microsphere, possibly because of the viscosity of NOA 61. As such, the resonator is overcoupled and the coupling efficiency may be decreased.

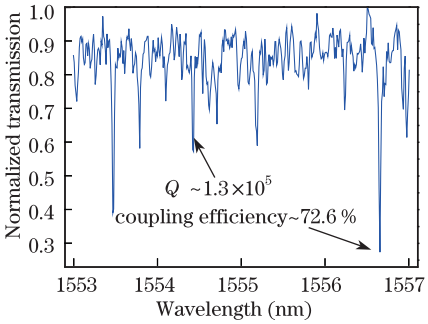

Fig. 5. Normalized transmission in the wavelength interval from 1553 to 1557 nm. Q: quality factor.

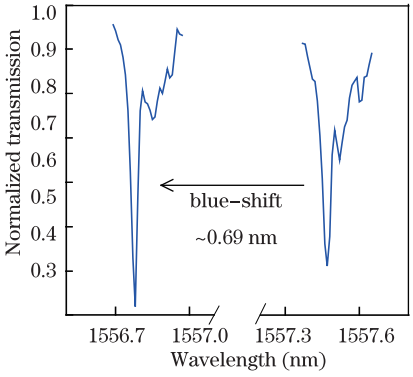

Fig. 6. Resonance peak shift with pump current from 250 to 500 mA.

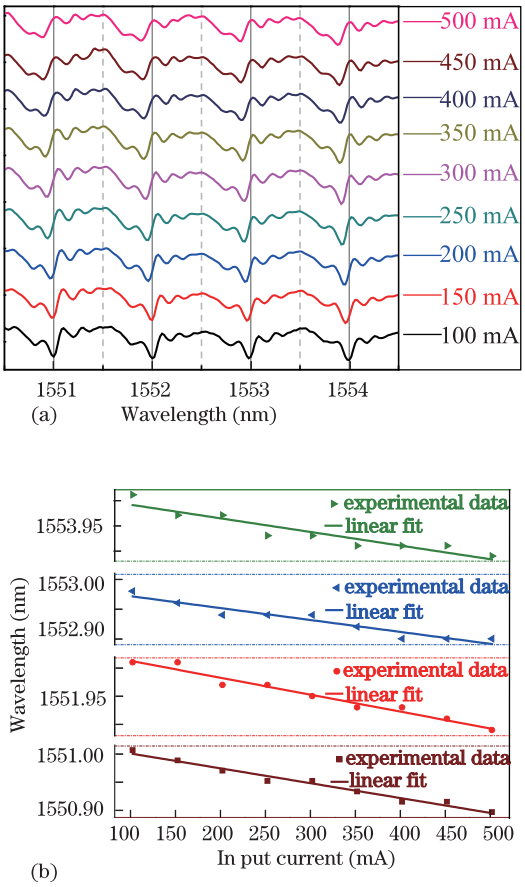

Fig. 7. (a) Transmission spectrum of the NOA 61 microsphere ($D \sim 499.4$ μm) under different input energies; (b) resonant wavelength shift of the four WGM peak positions as a function of input pump current.

The Q-factor of a microsphere resonator can be easily estimated by the resonance linewidth of the WGM spectrum, expressed as $Q{=}\lambda/\delta\lambda$, where λ is the central resonance wavelength and $\delta\lambda$ is the full-width at half-maximum (FWHM). By using the Lorentzian fit of the experimental data acquired from OSA, a FWHM of 11.6 pm at a central resonance wavelength of 1554.43 nm was found. The resonance Q-factor of the microsphere resonator is estimated to be $1.3{\times}10^5$. This measured value is limited by the OSA's resolution (0.01 nm), whereas the real Q-factor is likely to be higher. The real linewidth should be narrower than the resolution of the OSA, and the dip depth of resonance may be lower than the measurements. The coupling efficiency might also be higher.

In the experiment, a resonance peak experienced a blue shift of 0.69 nm when the pump current of the broadband light source was set to hop from 250 to 500 mA (Fig. 6). The thermal drift of resonance WGMs in a microsphere resonator results from the thermal-optic effects and thermal expansion of the microsphere material. The resonant wavelength shift $\Delta\lambda$ can be estimated as[23]

$$\Delta\lambda = \lambda\Big(\frac{1}{D}\frac{\mathrm{d}D}{\mathrm{d}T} + \frac{1}{n}\frac{\mathrm{d}n}{\mathrm{d}T}\Big)\Delta T, \qquad (3)$$

where λ is the resonance wavelength, $D = 2\pi a$, ΔT is the temperature variation of NOA 61 microsphere, and $(1/D)(\mathrm{d}D/\mathrm{d}T)$ and $\mathrm{d}n/\mathrm{d}T$ are the thermal expansion coefficient and thermal refraction coefficient respectively.

Given that the NOA 61 optical adhesive is a material of negative thermal expansion and thermo-optic coefficients, a temperature rise will decrease both the refractive index and the size. Therefore, the resonant wavelength will shift to a shorter wavelength according to Eq. (3).

Experiments were carried out on a larger microsphere to further demonstrate the phenomenon of WGM resonances of a NOA 61 microsphere blue shifting with increasing input light power. This microsphere had a diameter of 499.4 μm coupled with a tapered optical fiber of 3-μm waist diameter. A blue shift of the overall resonance WGMs by changing the input light power (ranging from 100 to 500 mA of the pump current, with a single step increment of 50 mA) can be clearly seen in Fig. 7(a). The resonant wavelength shifts of the four WGM peak positions are depicted in Fig. 7(b). The experiment data can be fitted by four linear decreasing lines, and the wavelength shifts of these four WGM peak positions can be calculated using the four linear-fitting formulas. When the input pump power increases from 250 to 500 mA, the computed peak position shifts are about 0.07, 0.069, 0.053, and 0.06 nm. These values are less than the wavelength shift of 0.69 nm in Fig. 6. The reason for this result is that the temperature change (ΔT) of the microsphere scales is $\Delta T \propto 1/l^2$, whereas l^2 is proportional to the surface area of the microsphere[24]. Considering the negative thermal expansion and thermo-optic coefficients of NOA 61, the resonant wavelength shifts is inversely proportional to the surface areas of the microspheres. In our experiment, the ratio of the resonant wavelength shifts and the ratio of surface areas of the two aforementioned microspheres with diameters of 160.6 and 499.4 μm are about 0.1 and 9.7 respectively. These values are almost exactly inversely proportional to each other. The results demonstrate a potential application of the UV-curable adhesive microsphere in thermal sensing and frequency tuning.

In conclusion, fabrication and characterization of UV-curable adhesive microspheres are demonstrated. Optical microspheres are produced with almost perfect sphericity by curing the liquid microdroplets of the optical adhesive (NOA 61) that adhere to the tip of half-tapered fibers using a 365-nm UV spot-curing system. WGMs of a microsphere are characterized experimentally and analyzed theoretically. Q-factors exceeding 10^5 near 1550 nm are observed. The WGM resonance shows a blue shift with increasing light power and temperature caused by the negative thermo-optic and thermal expansion effects of the material. These microspheres also have the advantages of low optical attenuation, low cost, and processing flexibility, which make them good alternatives for fabricating high-Q WGMRs and promising candidates for thermo-optic sensing and frequency tuning.

This work was supported by the National Natural Science Foundation of China (No. 61275050), the Specialized Research Fund for the Doctoral Program of Higher Education (No. 20120121110034), and the Fundamental Research Funds for the Central Universities of Xiamen University (Nos. 2010121059 and 2011121048).

References

1. C. C. Lam, P. T. Leung, and K. Young, J. Opt. Soc. Am. B **9,** 1585 (1992).
2. K. J. Vahala, Nature **424,** 839 (2003).
3. M. Sumetsky, Opt. Lett. **29,** 8 (2004).
4. Y. Huang, C. Guo, R. Bao, and X. Wang, Chin. Opt. Lett. **11,** 052201 (2013).
5. G. C. Righini, Y. Dumeige, P. Féron, M. Ferrari, G. N. Conti, D. Ristic, and S. Soria, Rivista Nuovo Cimento **34,** 435 (2011).
6. A. Chiasera, Y. Dumeige, P. Féron, M. Ferrari, Y. Jestin, G. Nunzi Conti, S. Pelli, S. Soria, and G. C. Righini, Laser Photon. Rev. **4**(3)**,** 457 (2010).
7. A. Ashkin and J. M. Dziedzic, Phys. Rev. Lett. **38,** 1351 (1977).
8. H. M. Tzeng, K. F. Wall, M. B. Long, and R. K. Chang, Opt. Lett. **9,** 499 (1984).
9. R. Symes, R. M. Sayer, and J. P. Reid, Phys. Chem. Chem. Phys. **6,** 474 (2004).
10. S. X. Qian and R. K. Chang, Phys. Rev. Lett. **56,** 926 (1986).
11. H. M. Tzeng, K. F. Wall, M. B. Long, and R. K. Chang, Opt. Lett. **9,** 273 (1984).
12. H. B. Lin, J. D. Eversole, and A. J. Campillo, Opt. Commun. **77,** 407 (1990).
13. V. B. Braginsky, M. L. Gorodetsky, and V. S. Ilchenko, Phys. Lett. A **137,** 393 (1989).
14. T. Ioppolo, U. K. Ayaz, M. V. Ötügen, and V. Sheverev, *46th AIAA Aero-space Sciences Meeting and Exhibit 2008* 273 (2008).
15. Y. F. Xiao, L. He, J. Zhu, and L. Yang, Appl. Phys. Lett. **94,** 231115 (2009).
16. C. H. Dong, L. He, Y. F. Xiao, V. R. Gaddam, S. K. Ozdemir, Z. F. Han, G. C. Guo, and L. Yang, Appl. Phys. Lett. **94,** 231119 (2009).
17. B. B. Li, Q. Y. Wang, Y. F. Xiao, X. F. Jiang, Y. Li, L. X. Xiao, and Q. H. Gong, Appl. Phys. Lett. **96,** 251109 (2010).
18. T. Ioppolo, M. Kozhevnikov, V. Stepaniuk, M. V. Ötügen, and V. Sheverev, Appl. Opt. **47,** 3009 (2008).
19. H. Li, L. Lei, Q. Zeng, J. Shi, C. X. Luo, H. Ji, Q. Ouyang, and Y. Chen, Sens. Actuators B Chem. **145,** 570 (2010).
20. Norland Products Inc., https://www.norlandprod.com/adhesives/NOA%2061.html
21. J. C. Knight, G. Cheung, F. Jacques, and T. A. Birks, Opt. Lett. **22,** 1129 (1997).
22. P. Wang, T. Lee, M. Ding, A. Dhar, T. Hawkins, P. Foy, Y. Semenova, Q. Wu, J. Sahu, G. Farrel, J. Ballato, and G. Brambilla, Opt. Lett. **37,** 728 (2012).
23. Z. Cai, A. Chardon, H. Xu, P. Féron, and G. M. Stéphan, Opt. Commun. **203,** 301 (2002).
24. J. Carmon, L. Yang, and K. J. Vahala, Opt. Express **12,** 4742 (2004).